

High-precision K-band photometry of the secondary eclipse of HD209458

I.A.G. Snellen^{1,2*}

¹ *Leiden Observatory, Postbus 9513, NL-2300RA Leiden, The Netherlands*

² *Institute for Astronomy, University of Edinburgh, Blackford Hill, Edinburgh, EH9 3HJ, UK*

ABSTRACT

Recently, mid-infrared Spitzer observations have been presented that show the light decrement due to the passage of a planet behind its host star. These measurements of HD209458b and TrES-1 are the first detections of direct light from an extra-solar planet. Interpretation of these results in terms of planet equipartition temperature and bond albedo is however strongly model dependent and require additional observations at shorter wavelengths. Here we report on two attempts to detect the secondary eclipse of HD209458b from the ground in K-band, using the UK InfraRed Telescope (UKIRT). A photometry precision of 0.12% relative to two nearby reference stars was reached during both occasions, but no firm detection of the eclipses were obtained. The first observation shows a flux decrement of $-0.13 \pm 0.18\%$, and the second of $-0.10 \pm 0.10\%$. A detailed description of the observing strategy, data reduction and analysis is given, and a discussion on how the precision in ground-based K-band photometry could be further improved. In addition we show that the relative photometry between the target and the reference stars between the two epochs is consistent down to the $<0.1\%$ level, which is interesting in the light of possible near-infrared surveys to search for transiting planets around M and L dwarfs.

Key words: eclipses - infrared:stars - planetary systems - stars:individual(HD209458) - techniques:photometric

1 INTRODUCTION

The large majority of the extra-solar planets known to date have been discovered using the radial velocity technique, providing a wealth of information on the orbital properties of the exoplanet population (e.g. Marcy et al. 2005). However, so far only those planets that *transit* their host star have given also an insight in the properties of the planets themselves. Firstly, the observations of the transit allows the determination of the inclination of the orbit, and subsequently the planetary mass, radius, and density. Furthermore, precise determination of the transit depth as function of wavelength can reveal atmospheric constituencies. For the brightest transiting exoplanet system known so far, HD209458b, this has resulted in the detection of Sodium in the exoplanet’s atmosphere (Charbonneau et al. 2002), and hydrogen, carbon, and oxygen in its evaporating exosphere (Vidal-Madjar et al. 2003; 2004)

Recently, observations of transiting exoplanet systems have resulted in a new breakthrough in exoplanet research. By observing secondary eclipses of the two brightest known

transiting exoplanets, HD209458 and TrES-1, the light contribution from the planets have been determined. While Charbonneau et al. (2005) observed a secondary eclipse of TrES-1 with Spitzer at 4.5 and 8 micron, Deming et al. (2005) targeted HD209458 (also with Spitzer) at 24 micron. The three flux measurements, showing relative contributions from 0.07% to 0.28%, are reasonably consistent with the expectations from emission models, confirming a basic understanding of hot Jupiter atmospheric physics (Seager et al. 2005; Burrows, Hubeny & Sudarsky 2005; Fortney et al. 2005). However, detailed conclusions can not be reached, and strong model degeneracies yet exist between e.g. the strength of molecular absorption, the Bond albedo, the redistribution of heat from the day to the night side of the planet, and the effective temperature of the planet.

To allow a more detailed interpretation in terms of planetary atmosphere physics and energy budgets, the flux measurements obtained so far ideally need to be complemented with observations at shorter wavelengths. In particular, new measurements would be valuable from around the peak of the planets’ energy distributions, between H₂O absorption bands at 1–4 μm . Although here the planet/star flux ratio is in general less favourable than at longer wavelengths,

* E-mail: snellen@strw.leidenuniv.nl

Table 1. Data on the exoplanet system HD209458, and two nearby stars used for flux calibration. The near-infrared data are extracted from the 2MASS point source catalogue. The data on HD209458b is taken from the extra-solar planet encyclopedia (<http://www.obspm.fr/encycl/encycl.html>).

| |
|---|
| HD209458 (2MASS22031077+1853036) |
| <i>Stellar data</i> |
| Distance = 47 pc |
| Spectral type = G0V |
| Mass = 1.05 M_{sun} |
| Radius = 1.12 R_{sun} |
| Metallicity = 0.04 [Fe/H] |
| $K_{2\text{MASS}}=6.591$ |
| $J-K_{2\text{MASS}}=0.283$ |
| <i>Planet data</i> |
| Mass = $0.69 \pm 0.05 M_{\text{Jup}}$ |
| Radius = $1.32 \pm 0.05 R_{\text{Jup}}$ |
| Orbital Period = $3.52474541 \pm 0.00000025$ days |
| T_0 (Mid-transit) = $2\,452\,854.825415 \pm 0.000060$ |
| Semi-major axis = 0.045 AU. |
| REF. A (2MASS22030745+1851343) |
| $K_{2\text{MASS}}=9.912$ |
| $J-K_{2\text{MASS}}=0.310$ |
| REF. B (2MASS22031559+1855064) |
| $K_{2\text{MASS}}=8.853$ |
| $J-K_{2\text{MASS}}=0.769$ |

strong peaks in the spectral energy distribution of the planet around 2.2 and 3.9 μm are expected to significantly boost the signal, resulting in possible planet/star flux ratios at a 0.1% level. This makes it potentially possible to observe the secondary eclipse from the ground. So far, the highest accuracy from the ground has been obtained using ‘occultation spectroscopy’ on HD209458b (Richardson et al. 2003a,b), aiming to detect the disappearance and reappearance of spectral features. This technique is sensitive only to the prominence of spectral features, not to the total flux of a planet. Their strongest limit has been obtained on the contrast of the 2.2 μm peak, at a level of $\sim 3 \times 10^{-4}$ of the stellar flux.

In this paper we present K-band photometry of the secondary eclipse of HD209458 obtained with UKIRT. To achieve a photometric precision of 0.1%, several challenges had to be overcome, in particular saturation of the K=6.3 star on the array, and non-linearity/aperture correction issues. The observation strategy and data reduction are described in sections 2 & 3, and the results and discussion are presented in sections 4 & 5.

2 OBSERVATIONS

We performed our K-band photometry on HD209458 with the 3.8m United Kingdom Infrared Telescope (UKIRT) on Mauna Kea, Hawaii, using UIST, the UKIRT 1-5 micron Imager Spectrometer. HD209458b is of K=6.30 (see table 1), which means that under good seeing conditions it saturates the array within the shortest possible exposure time. It was therefore necessary to significantly defocus the telescope. UIST is equipped with a 1024x1024 InSb array, but only one quadrant was used to reduce readout times. In

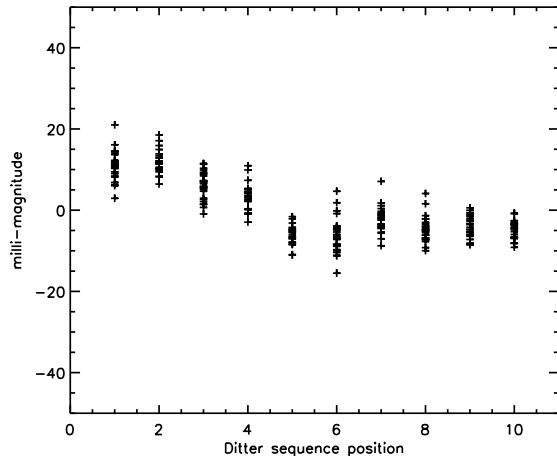


Figure 1. The relative K-band flux of HD209458b as function of the position in the jitter sequence for the observations obtained on September 13, 2004.

small pixel mode ($0.06''/\text{pixel}$) this results in a field of view of 30×30 arcseconds. Observing cycles of 15 minutes were defined in which subsequently the target, a reference star ref_A , again the target, and reference star ref_B were observed. Each observation consists of a repeated 5-point jitter (with $\pm 8''$ offsets in RA and DEC), with the target and the reference stars falling onto the same area of the array. The reference stars ref_A and ref_B are 2MASS22030745+1851343 and 2MASS22031559+1855064, at a distance of $101''$ and $140''$ to HD209458b respectively (see table 1 for details). The data were taken in NDSTARE mode, in which the array is reset, read immediately, and read again after the user-defined on-chip exposure time. Exposure times were 0.6, 6.0, and 3.0 seconds for the target, ref_A , and ref_B respectively.

Observations for this project were taken on three dates, all taken in service mode. Firstly, 1 hour test observations were performed on July 21, 2004 to check the observing settings. Subsequently, HD209458b was observed on August 23, from 06:06 UT to 10:18 UT, during which the eclipse occurred in the first half of the observation (assuming a circular orbit for HD209458b). The dome had to be briefly closed due to local fog. The target was observed again on the night of September 13, from 07:22 UT to 11:27 UT. Here the eclipse occurred during the second part of the observations. A series of blank sky observations were used to construct a flat field at each epoch.

3 DATA REDUCTION

Data reduction and analysis was performed in IDL. Firstly, a non-linearity correction was applied to the data, using the predetermined relation,

$$g' = (1 + 8.26 \times 10^{-5}g - 1.56 \times 10^{-8}g^2 + 1.173 \times 10^{-12}g^3) * g(1)$$

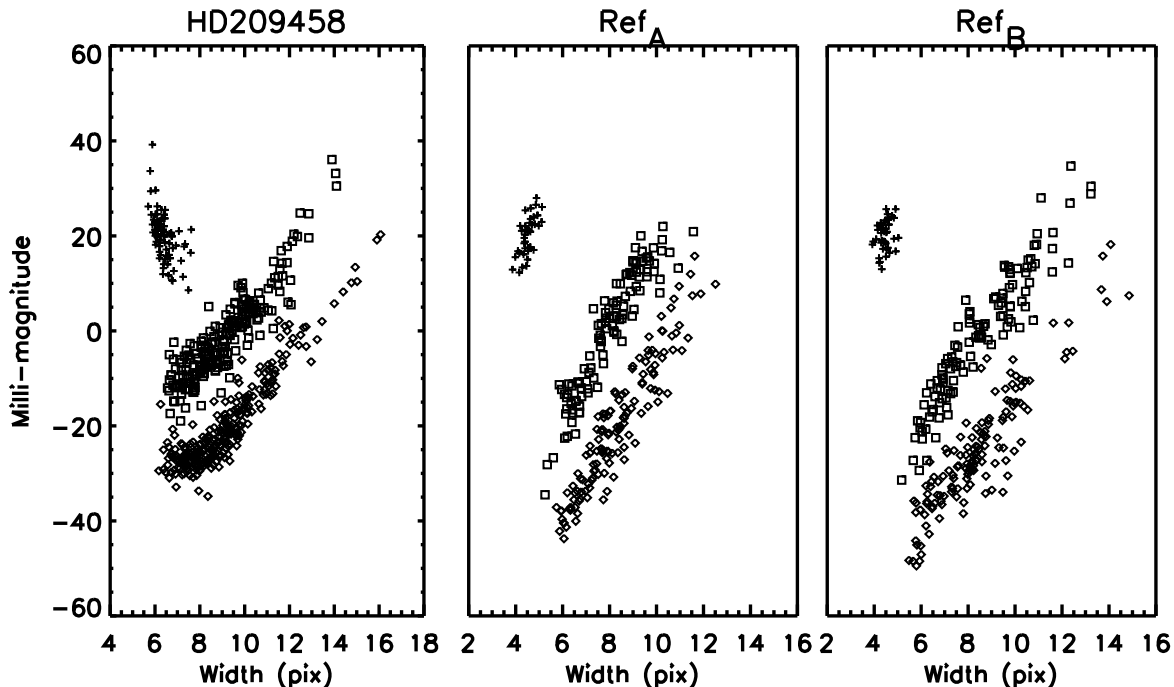


Figure 2. The relative flux density of HD209458b (left), Ref_A (middle) and Ref_B (right) as function of the profile-width, for the July (crosses), August (squares), and September (diamond) observations. The data-sets have been given separate offsets for clarification. The dependencies are clearly different for the three sources, and most likely result from an interplay between residual non-linearity and aperture effects.

where g and g' are the measured and corrected data values (Sandy Leggett, privat communications). A dark was subtracted from each individual frame, after which it was divided through the flat field. The sky background was determined in the following way. First those areas on the array were identified that are sufficiently away from the object at all jitter positions. The median background level in this area was determined for each frame, through which the frame was then normalised. These normalised frames were then used to determine any structure in the background by first masking out the object and then combining them. The resulting image was then multiplied by the median background level as determined above, to yield a sky-frame for each jitter point. This resulted in a dark subtracted, flat fielded, and sky subtracted frame for each jitter point.

For each frame the total counts from the object was determined within a radius of 30, 40, 50, 60, and 70 pixels from its centre. In addition, a one-dimensional profile of the object was determined and fitted with a Lorentzian function, which was found to fit well. A first-order aperture correction was applied, as calculated from that part of the 2-dimensional Lorentzian profile to fall outside the aperture, and the counts were converted to instrumental magnitudes. A small fraction (1-2%) of the data points were not taken into account for further analysis, since their frames showed clear anomalies such as highly irregular light profiles indicating that the telescope underwent tracking errors during the exposure.

4 RESULTS AND ANALYSIS

The test observations of July 2004

The data taken on July 21 consists 4 cycles of target-ref_A-target-ref_B, resulting in 80 data frames for HD209458b, and 40 frames for each of the reference stars. The data points, determined as described above, show a scatter of 22.6 milli-magnitude, but show a clear pattern (such as shown in Fig. 1). Firstly there is a clear dependence on jitter point, the first data point being on average 23 milli-magnitude fainter than the last data point in the jitter sequence. It is not clear what is causing this, but since it is found to be constant in time, it can be calibrated out. Secondly, there is a clear dependence of the magnitude of a data point on the width of the Lorentzian as fitted above. This dependence was found to be different for the target and the two reference stars (see the 'cross' symbols in Fig. 2). The relation between profile-width and magnitude for the target is such that the narrower the profile, the fainter the magnitude. This indicates that it may be caused by a residual non-linearity effect, but residual aperture correction effect may also play a role. The dependence between profile-width and magnitude goes the other way around for ref_A and ref_B. This different behaviour may be due to the fact that these objects were observed at lower count levels than the target, resulting in a different interplay between non-linearity and aperture correction effects. Note that the star profiles during the August and September observations (squares and diamonds in Fig. 2) have sig-

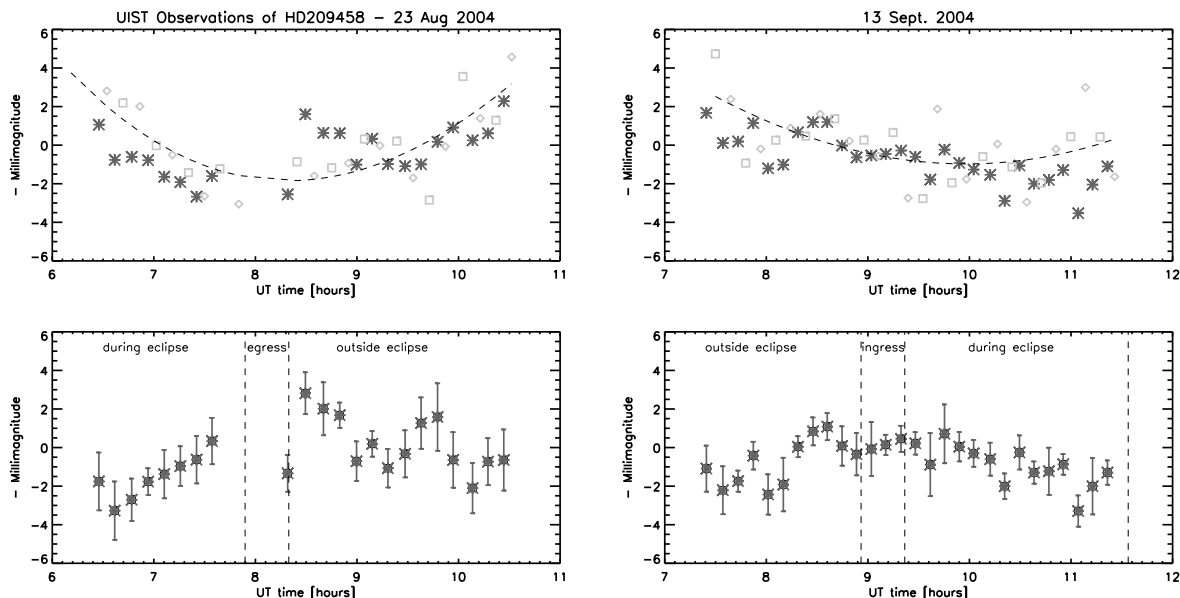


Figure 3. (left) The relative photometry obtained on August 23, 2004. The upper panel shows the data for the target (stars), ref_A (squares), and ref_B (diamonds). The dashed line shows the fit to the change in zero-point as function of time, as determined from the two reference stars, which is used to determine the relative photometry for HD209458 as shown in the lower panel. The same data are shown for the September observations in the panels to the right.

nificantly broader widths, for which the width-magnitude relation of the target and reference stars do have the same sign. The width-magnitude relations for the target and the reference stars are fitted in an ad-hoc way. This results in a standard deviation of 5.3, 3.0, and 3.1 milli-magnitude for the target, ref_A and ref_B respectively.

The observations of August 2004

Assuming that HD209458b has a circular orbit for which the secondary eclipse occurs exactly halfway between two transits, HD209458b was mid-eclipse on August 23, 2004 at 6:47 UT (taking into account light travel time in our solar system). Twelve cycles of target- ref_A -target- ref_B were observed on that night from 06:06 UT to 10:18 UT. A similar pattern in magnitude as function of jitter position as found in July, was removed from the data. A new complication compared to the test observations was a significant change in airmass over the four hours of observations. Therefore the flux zero-point changed slowly causing a difference of 31 milli-magnitude between the beginning and the end of the observations. An airmass correction was determined for ref_A and applied to all three objects. The star profiles were found to vary more wildly between frame to frame than during the test observations, with the widths varying from 6 to 15 pixels. Since the variation was quasi-random with time, the width-magnitude relations for the target and the reference stars could be fitted and used to correct their magnitude in a similar way as for the test observations (but see below). When the corrections for airmass and profile width are applied, they result in an improved correction for jitter position, which in its way results in a better correction as function of airmass and profile width – and so forth. This iterative process quickly results in optimal solutions for all three relations, resulting in a dispersion of 3.6, 4.1, and 4.6

milli-magnitude for the target, ref_A and ref_B respectively. The 10 data points of each jitter sequence of each source are averaged to increase the signal-to-noise. The resulting photometry is shown in figure 3, with the lower panel showing the target data points relative to those of the two reference stars. For a circular orbit it is expected that the planet would reappear from behind its host star between 7:46 and 8:10 UT. The data points of HD209458 before this time are on average 1.4 ± 2.0 millimagnitude fainter ($-0.13 \pm 0.18\%$) than those after.

The observations of September 2004

On September 13, HD209458b underwent a secondary eclipse centered at 10:13 UT. Fourteen cycles of target- ref_A -target- ref_B were observed on that night from 07:22 UT to 11:27 UT. A similar pattern in magnitude as function of jitter position was found as for the two epochs before, and removed from the data. While these observations were more ideally timed, with the objects located at low airmass throughout the observing session, the seeing dramatically improved during the four hours of observing, causing the profile-widths to change from on average of 14.5 pixels in the third cycle, to 7.0 pixels in the last cycle. This resulted in a degeneracy between a possible flux density change from the first to the second half of the data set for HD209458 (as expected for an eclipse), and the precise relation between seeing and measured flux density. Indeed, if a fake signal is introduced that mimics an eclipse, the reduction procedure as described above subsequently removes most of it. This problem was solved by fitting the width-magnitude relation for the in- and out-eclipse data separately, allowing a flux offset between the two relations but keeping the flux-dependence on width the same for the two sub-sets, hence adding one extra variable. In this way the reduction pro-

cedure leaves a fake signal intact. Note that analysing the August dataset in this way does not change the result obtained above. The in-eclipse flux points are found to be on average 1.1 ± 1.1 milli-mag fainter ($-0.10 \pm 0.10\%$) than outside the eclipse (see Fig. 3).

5 DISCUSSION AND CONCLUSIONS

Our observations of the secondary eclipse of HD209458b have resulted in a photometric accuracy of $\sim 0.12\%$ per 15 min. cycle compared to two nearby reference stars. No firm detections of the eclipses were obtained, with the first observation showing a flux decrement of $-0.13 \pm 0.18\%$ during the time of the eclipse, and the second of $-0.10 \pm 0.10\%$. In Fig. 4 we show the combined dataset. Note that the average brightness-difference between the two reference stars and HD209458 changed by only ~ 0.3 milli-magnitude between the two epochs and was not corrected for. An eclipse-profile was fitted to this combined dataset, for a circular orbit (solid line), and for a non-circular orbit (dotted line), allowing the precise timing of the eclipse to change. This because a non-zero orbital eccentricity can produce a shift in the separation of the times of transit and eclipse away from half-period, although Deming et al (2005) find that the secondary eclipse of HD209458 occurs at the mid-point between transits to within ± 7 minutes. Neither the fit for a fixed circular orbit, nor the fit for a free eclipse time give a significantly better fit than obtained for the individual data sets. By eye, one may be inclined to see a hint of an eclipse, but the uncertainty in the average flux level outside the eclipse (combined with the uncertainty in the flux offset between the two datasets) makes this signal not statistically significant.

Figure 5 shows a model of the eclipse depth as function of wavelengths for HD209458b, as calculated by Sudarsky, Burrows, & Hubeny (2003), scaled to fit the $24 \mu\text{m}$ measurement by Deming et al. (2005). Over-plotted are also the two eclipse-depth measurements of Charbonneau et al. (2005) for TrES-1, which is expected to show very similar eclipses. It shows that for this baseline model, at $2.2 \mu\text{m}$ an eclipse-depth of ~ 1 milli-magnitude is expected, while the observations described in this paper provide an upper limit of ~ 2.1 milli-magnitude. Note that Richardson et al. (2003), who used occultation spectroscopy to measure the strength of the feature at $2.2 \mu\text{m}$, claim to detect no such peak at a level of $\sim 3 \times 10^{-4}$ of the stellar flux, rejecting the Sudarsky et al. baseline model.

Future prospects

We believe there are several ways to further improve the relative photometric precision of ~ 1 milli-magnitude as obtained here. First of all, HD209458 is not anymore the most ideal candidate for ground-based photometry.¹ TrES-1 (discovered in August 2004; Alonso et al. 2004) is of $K=9.8$, with two nearby stars with similar magnitudes and colours.

¹ The referee, Drake Deming, instead suggests to monitor HD209458 with a smaller aperture telescope, avoiding saturation and allowing to simultaneously observe bright comparison stars in its wider field of view.

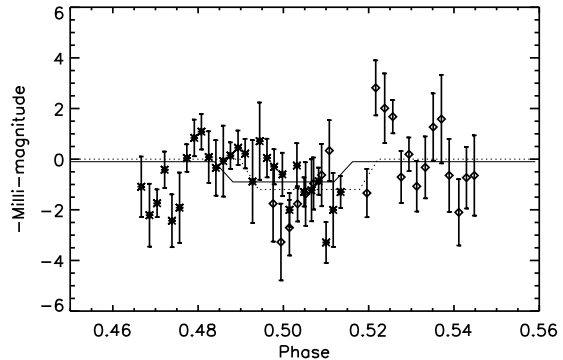


Figure 4. The combined dataset for the August 23 (diamonds) and September 13 (stars) observations. Note that no flux offset was applied between the two datasets. The solid line indicates the best fitting eclipse for a fixed circular orbit, and the dotted line while keeping the eclipse timing as a free parameter. The combined flux decrement is not statistically significant due to the uncertainty in the flux-level outside the eclipse, and the uncertainty in the flux offset between the two datasets.

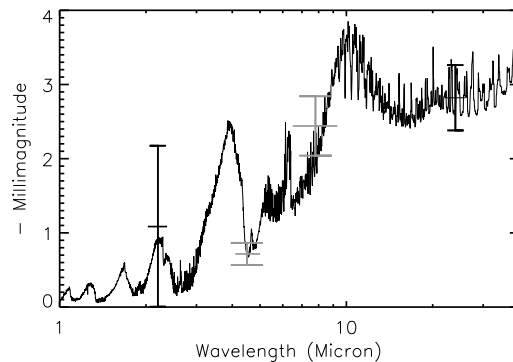


Figure 5. Eclipse depth as function of wavelength for HD209458, assuming the baseline model-atmosphere as determined by Sudarsky et al. (2003), but scaled to the eclipse-depth measurement of Deming et al. (2005) at $24 \mu\text{m}$. The two grey data points indicate the measurements from Charbonneau et al. (2005) of the exoplanet system TrES-1 (which flux ratios are not expected to differ much from that of HD209458).

This means that the telescope does not have to be defocused and that the aperture correction problems may be less prominent. Furthermore, for TrES-1, the nearby stars mean that the calibrators can be observed in the same frame as the target, which we believe will improve the photometry considerably. Frame-to-frame variations in the observations for HD209458b indicate that, if a perfect calibration of the throughput of the telescope+atmosphere and the sensitivity of the array had been possible, a further improvement of 30-40% in precision would be possible. Furthermore, observing the complete eclipse, plus a significant period before and after the dis- and reappearance of the planet would allow possible slowly varying drifts in flux density, e.g. due to intrinsic variability of calibrations stars.

In addition to secondary eclipse observations, high precision near-infrared photometry has also a potentially inter-

esting application in exoplanet transit surveys, in particular in the light of the recent advent of large infrared arrays such as WFCAM on UKIRT, WIRCam on the CFHT, and in the near future, VISTA. We show that relative photometry in K-band is possible down to a milli-magnitude level. Near-infrared transit surveys are particularly interesting for probing planets around late M and L dwarfs, which are significantly brighter in K-band than in the optical. Their relatively small size will make any planet transit more pronounced than for solar type stars. For example, a transit of an earth size planet around an M8 dwarf star ($R \sim 0.2R_{\text{sun}}$), would result in a transit depth of $\sim 0.2\%$. Hence, it may potentially be possible to detect earth-type planets with near-infrared transit surveys.

ACKNOWLEDGEMENTS

The author wishes to thank the UKIRT staff, in particular Andy Adamson and Sandy Leggett, for their help and suggestions during the project. Also thanks to Katherine Inskip for doing the September observations in service. The United Kingdom Infrared Telescope is operated by the Joint Astronomy Centre on behalf of the U.K. Particle Physics and Astronomy Research Council.

REFERENCES

- Burrows A., Hubeny I., & Sudarsky D., 2005, ApJ 625, L135
- Charbonneau D., Brown T.M., Noyes R.W., Gilliland R.L., 2002, ApJ 568, 377
- Charbonneau D., Allen L., Megeath S., Torres G., Alonso R., Brown T., Gilliland R., Latham D., Mandushev G., O'Donovan F., Sozzetti A., 2005, ApJ, accepted
- Deming D., Seager S., Richardson J. & Harrington J. 2005, Nature , 434 , 740
- Fortney J.J., Marley M.S., Lodders K., Saumon D., Freedman R., 2005, ApJ 627, L69
- Marcy G., Butler R.P., Fischer D., Vogt S., Wright J.T., Tinney C.G., Jones H.R.A, 2005, Progress of Theoretical Physics Supplement, in press
- Richardson, L. J., Deming, D., Wiedemann, G., Goukenleuque, C., Steyert, D., Harrington, J., & Esposito, L. W., 2003a, ApJ, 584, 1053
- Richardson J.L., Deming D., Seager S., 2003b, ApJ 597, 581
- Seager S., Richardson L.J., Hansen B.M.S., Menou K., Cho J.Y-K., Deming D., 2005, submitted to ApJ
- Sudarsky D., Burrows A., & Hubeny I., 2003, ApJ 588, 1121
- Vidal-Madjar A, Lecavelier des Etangs A., Désert J.-M., Ballester G.E., Ferlet R., Hébrard G., Mayor M., Nature 422, 143
- Vidal-Madjar A, Désert J.-M., Lecavelier des Etangs A., Hébrard G., Ballester G.E., Ehrenreich D., Ferlet R., McConnell J.C., Mayor M., Parkinson C.D., 2004, ApJL submitted